



RESEARCH ARTICLE

Raman needle arthroscopy for in vivo molecular assessment of cartilage

Kimberly R. Kroupa¹ | Man I Wu¹ | Juncheng Zhang² | Magnus Jensen³ |
Wei Wong¹ | Julie B. Engiles⁴ | Thomas P. Schaer⁵ | Mark W. Grinstaff^{2,6}  |
Brian D. Snyder⁷ | Mads S. Bergholt³ | Michael B. Albro^{1,6} 

¹Department of Mechanical Engineering, Boston University, Boston, Massachusetts, USA

²Department of Biomedical Engineering, Boston University, Boston, Massachusetts, USA

³Department of Craniofacial Development & Stem Cell Biology, Kings College, London, UK

⁴Department of Pathobiology, New Bolton Center, University of Pennsylvania, Kennett Square, Pennsylvania, USA

⁵Department of Clinical Studies, New Bolton Center, School of Veterinary Medicine, University of Pennsylvania, Philadelphia, Pennsylvania, USA

⁶Division of Materials Science & Engineering, Boston University, Boston, Massachusetts, USA

⁷Department of Orthopaedic Surgery, Boston Children's Hospital, Boston, Massachusetts, USA

Correspondence

Mads S. Bergholt, Department of Craniofacial Development & Stem Cell Biology, Kings College London, UK.

Email: mads.bergholt@kcl.ac.uk

Michael B. Albro, Department of Mechanical Engineering, Boston University, Boston, Massachusetts, USA.

Email: albro@bu.edu

Funding information

Arthritis Foundation; H2020 European Research Council, Grant/Award Number: 802778; Musculoskeletal Transplant Foundation

Abstract

The development of treatments for osteoarthritis (OA) is burdened by the lack of standardized biomarkers of cartilage health that can be applied in clinical trials. We present a novel arthroscopic Raman probe that can “optically biopsy” cartilage and quantify key extracellular matrix (ECM) biomarkers for determining cartilage composition, structure, and material properties in health and disease. Technological and analytical innovations to optimize Raman analysis include (1) multivariate decomposition of cartilage Raman spectra into ECM-constituent-specific biomarkers (glycosaminoglycan [GAG], collagen [COL], water [H₂O] scores), and (2) multiplexed polarized Raman spectroscopy to quantify superficial zone (SZ) COL anisotropy via a partial least squares–discriminant analysis-derived Raman collagen alignment factor (RCAF). Raman measurements were performed on a series of ex vivo cartilage models: (1) chemically GAG-depleted bovine cartilage explants ($n = 40$), (2) mechanically abraded bovine cartilage explants ($n = 30$), (3) aging human cartilage explants ($n = 14$), and (4) anatomical-site-varied ovine osteochondral explants ($n = 6$). Derived Raman GAG score biomarkers predicted 95%, 66%, and 96% of the variation in GAG content of GAG-depleted bovine explants, human explants, and ovine explants, respectively ($p < 0.001$). RCAF values were significantly different for explants with abrasion-induced SZ COL loss ($p < 0.001$). The multivariate linear regression of Raman-derived ECM biomarkers (GAG and H₂O scores) predicted 94% of the variation in elastic modulus of ovine explants ($p < 0.001$). Finally, we demonstrated the first in vivo Raman arthroscopy assessment of an ovine femoral condyle through intraarticular entry into the synovial capsule. This study advances Raman arthroscopy toward a transformative low-cost, minimally invasive diagnostic platform for objective monitoring of treatment outcomes from emerging OA therapies.

KEYWORDS

articular cartilage, imaging, osteoarthritis diagnostics, Raman spectroscopy

Kimberly R. Kroupa, Man I Wu, and Juncheng Zhang contributed equally to this study.

[Correction added after first publication on 20 December 2021: The order of authors in the author byline were revised by Adding new author name “Thomas P. Schaer”.]

This is an open access article under the terms of the Creative Commons Attribution-NonCommercial-NoDerivs License, which permits use and distribution in any medium, provided the original work is properly cited, the use is non-commercial and no modifications or adaptations are made.

© 2021 The Authors. *Journal of Orthopaedic Research*® published by Wiley Periodicals LLC on behalf of Orthopaedic Research Society.

1 | INTRODUCTION

Osteoarthritis (OA) is a chronic, debilitating condition, characterized by the progressive degradation of articular cartilage. It is the most widespread cause of disability in adults; over 20% of the US adult population (>50 million individuals) is afflicted with the disease, with this number predicted to rise sharply over coming decades.^{1,2} Currently, no Food and Drug Administration approved therapies exist that reliably mitigate the degradation of cartilage tissue properties induced by OA.

The structure and composition of articular cartilage are optimized for its mechanical performance. It is comprised of a type-II collagen (COL) fibril network that affords structure and tensile strength, complemented by a negatively charged sulfated glycosaminoglycan (GAG) matrix that provides compressive properties and retains interstitial water.³ More than 90% of the applied joint load is supported by pressurization of entrapped water (interstitial fluid load support), yielding the tissue's characteristic low frictional properties.⁴ In addition, cartilage is inhomogeneous and structurally anisotropic, where the COL configuration varies with depth, segregated into zones optimized for mechanical performance: *superficial zone (SZ)*—comprised of COL fibers arranged parallel to the articular surface, *middle zone (MZ)*—mix-aligned COL, and *deep zone (DZ)*—perpendicular arranged COL. During OA, the GAG and COL constituents of the cartilage matrix become depleted, leading to compromised mechanical tissue function. Early on, GAG is depleted from the SZ^{5,6} with concomitant loss of superficial COL fiber organization and alignment.^{7,8} Loss of GAG and COL alignment reduces fluid load support, transferring loads to the COL matrix, and leading to cartilage erosion through the MZ and DZ. Later stages of OA progression are characterized by further GAG depletion and surface delamination, culminating in significant cartilage volume loss until bone-on-bone contact is reached.⁹

Numerous potential strategies to mitigate, protect, or regenerate the material properties of articular cartilage are emerging, including (1) modified joint kinetics (e.g., weight loss,¹⁰ physical therapy¹¹), (2) disease-modifying OA drugs,¹² (3) viscosupplements,¹³ and (4) surgically assisted tissue regeneration (microfracture, chondrocyte implantation, stem cell therapies).¹⁴ However, the ability to assess the efficacy of OA treatments that preserve and/or regenerate cartilage tissue structure and function is burdened by a lack of standardized biomarkers that can be applied in preclinical and clinical trials. Notably, clinical trials evaluating the efficacy of therapies rely on patient pain and mobility (WOMAC) scores that can be contaminated by the placebo effect and often correlate poorly to objective metrics of cartilage composition and structure. Image-based assessments (radiographs and magnetic resonance imaging [MRI]) are biased toward late-stage OA pathoanatomy (cartilage volume loss, bone marrow edema, cysts, and osteophytes). MRI measurements of cartilage composition and structure may be affected by lack of consistency, signal-to-noise ratio (SNR), and insufficient image resolution.

Raman spectroscopy is predicated on the inelastic scattering of photons. When monochromatic laser light induces a change in molecular polarizability during vibrations, a small proportion of the

incident photons (~ 1 in 10^8) is scattered with a change in wavelength.¹⁵ The Raman scattered light reflects the vibrational modes of constituent molecules; the absorbed energy corresponds to specific Raman active vibrational modes that define a molecule's "fingerprint." Thus, Raman spectra carry information about individual molecular vibrational bonds that correspond to specific biochemical building blocks (amides, sulfates, carboxylic acids, hydroxyls) of key cartilage constituents (GAG, COL, H₂O). The premise of this study is that Raman spectroscopy can "optically biopsy" cartilage and quantify the relative contribution of key constituents that serve as biomarkers for determining cartilage composition, structure, and material properties in health and disease. Prior work has demonstrated that Raman spectra of cartilage exhibit statistical changes in response to mechanical damage^{16–18} and OA.^{19–22} However, the implementation of Raman spectroscopy as a diagnostic tool for cartilage health has been impeded by a lack of clinically compatible intra-articular Raman probes for in vivo diagnostics and an inability to extract specific and quantitative biochemical and structural metrics related to cartilage health.

In this study, we develop a clinically compatible Raman needle arthroscopy platform for in vivo molecular assessment of cartilage. A thin, fiber-optic Raman spectroscopic probe, which can be directed intra-articularly via a hypodermic needle-cannula, was developed to "optically biopsy" cartilage at specific anatomic sites under image guidance. Technological and analytical innovations to optimize Raman spectral analysis include (1) decomposing composite Raman cartilage spectra and isolating the relative contribution of specific cartilage constituents, and (2) using multiplexed polarized Raman spectroscopy to quantify SZ COL anisotropy. We first establish the potential of our Raman arthroscopic probe to measure composition, structure, and material properties of cartilage that undergo changes during OA through parametric analysis of a series of ex vivo model systems: (1) Raman quantification of GAG content in enzymatically depleted bovine cartilage and aging human cartilage explants, (2) Raman quantification of zonal COL network organization in mechanically abraded bovine cartilage explants, and (3) Raman measurements of bovine cartilage thickness. Subsequently, we assess the ability of Raman biomarkers to predict the composition, thickness, and mechanical properties of cartilage explants from different anatomical sites of an ovine knee joint. We finally perform an in vivo Raman arthroscopic assessment of the composition of an ovine femoral condyle, demonstrating the clinical feasibility of Raman OA diagnostics.

2 | METHODS

2.1 | Raman needle arthroscopic probe instrumentation

A custom polarized Raman needle arthroscopic probe was developed for in vivo OA diagnostics by intra-articular entry through a hypodermic needle (Figure 1A–C)²³ (described in Supporting Information Material).

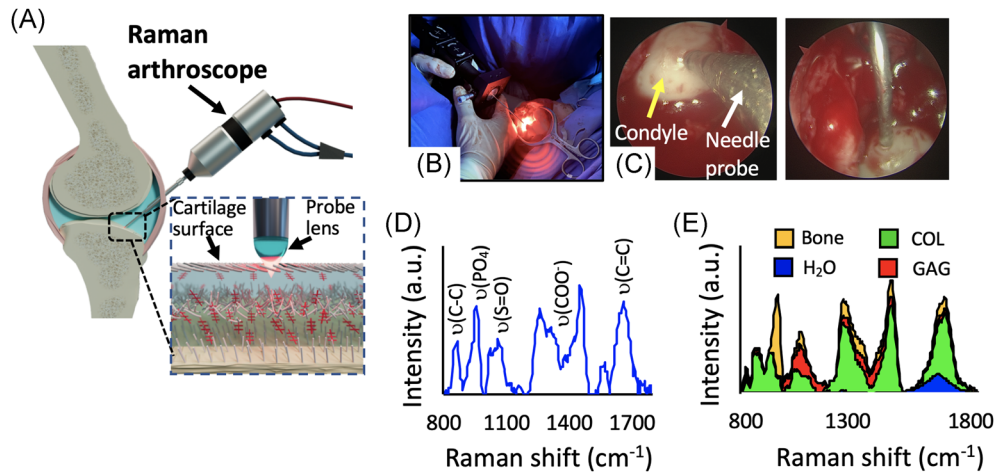


FIGURE 1 In vivo Raman arthroscopy diagnostics. (A) Schematic of fiber-optic Raman needle arthroscopy probe for osteoarthritis diagnostics. The Raman spectroscopy system consists of a near-infrared (NIR) laser, a spectrometer with an NIR deep depletion CCD, and a novel needle Raman probe that enables simultaneous acquisition of both the parallel and perpendicular polarized Raman signal. (B) In vivo Raman spectroscopy assessment of ovine stifle joint. (C) Raman probe in direct contact with femoral condyle as visualized by the arthroscopic camera. (D) Raman spectra acquired in vivo of ovine femoral condyle articular cartilage. (E) Two-dimensional stacked area graph showing the contribution of GAG, COL, H₂O, and subchondral bone to composite ovine cartilage Raman spectra after multivariate linear regression (described in Section 2) [Color figure can be viewed at wileyonlinelibrary.com]

2.2 | Multivariate analysis

The Raman spectral contribution of GAG and water is characteristically “buried” under the much stronger COL signal (Figure S1), thereby obscuring the assessment of tissue GAG and H₂O content. Here, we build upon our prior work on multivariate spectral analysis by decomposing and isolating the relative contribution of the major cartilage extracellular matrix (ECM) constituents (GAG, COL, and H₂O) to the Raman cartilage spectra using regression coefficients derived from the multivariate least squares regression analysis:

$$\text{Cartilage}_{\text{spectra}} = \text{GAG}_{\text{score}} \times (\text{GAG}_{\text{REF}}) + \text{COL}_{\text{score}} \times (\text{COL}_{\text{REF}}) + \text{H}_2\text{O}_{\text{score}} \times (\text{H}_2\text{O}_{\text{REF}}), \quad (1)$$

where GAG_{REF}, COL_{REF}, and H₂O_{REF} are the component spectra of purified reference chemicals of each ECM constituent (Figure S1). The GAG_{score}, COL_{score}, and H₂O_{score} “scores” are the regression coefficients that reflect the contribution of the spectra of each constituent element to the cumulative Raman cartilage spectra.

2.3 | Raman probe GAG quantification ex vivo

The capability of our Raman arthroscopic probe and multivariate analysis to portray cartilage GAG content was assessed. Capitalizing on low ECM compositional heterogeneity,²⁴ DZ cartilage was extracted from explants (Ø5 ± 0.8 mm) of femoral condyle hyaline cartilage of 2-month-old calves (Green Village Packing Co.; N = 5 animals). To simulate the progressive loss of GAG, as observed in OA, explants were subjected to stepwise GAG depletion using timed exposure (0, 4, 24, or 48 h; n = 10

explants per group) of 4 M guanidine hydrochloride (GuHCl). Overnight exposure to 3 mg/ml hyaluronidase (HAase; 37°C and pH 6.0) produced full GAG depletion. Raman spectra were acquired on the central region of each explant using a convex lens and compared to the GAG, COL, and H₂O content and equilibrium compressive Young’s modulus (E_γ) of a Ø3 mm central core.

2.4 | Raman probe depth selective GAG quantification ex vivo

As cartilage degeneration occurs in a depth-dependent manner, initiating predominantly in the topmost regions of the tissue, we next investigated how depth selectivity affects the quantification of GAG using a shallow focusing lens (needle and Ø2 mm ball lens) and deep focusing lens (convex lens) (Figure S2). To induce progressive depth-dependent GAG reduction, mimicking OA progression, full-thickness bovine cartilage explants (Ø6 mm) were treated with 500 µg/ml trypsin (pH 7.2 at 4°C) for 0, 0.5, 2, 4, or 8 h (n = 4 explants per group). Raman spectra were acquired at the articular surface using the ball lens and convex lens. Subsequently, explants were fixed, paraffin-embedded, sectioned, and stained with Safranin O–fast green (SOFG). Safranin O colorimetric profiles were mapped through the depth using the red channel intensity and normalized to the average intensity at the 1.5 mm depth position. For each lens, profiles were multiplied by the depth of penetration (DOP) decay curves (see Section 3) and integrated through the tissue depth, yielding the colorimetric-based GAG content within the lens-specific Raman measurement window. For each lens, colorimetric GAG was compared to Raman GAG scores. On a separate batch of trypsin-digested explants, the indentation elastic modulus of the cartilage surface was compared to Raman GAG scores acquired with the ball lens.

2.5 | Raman probe GAG quantification in human cartilage ex vivo

To establish the clinical relevance of the derived Raman GAG scores, Raman needle probe measurements were performed on Ø4.0 mm chondral explants ($n = 13$) excised from the distal femoral condyles of three cadaveric human knees (NDRI; age/sex: 70/♀, 75/♂, 65/♀; 4–5 explants per donor). Specimens exhibited an average thickness of 1.1 ± 0.4 mm and no visual signs of surface damage or fibrillation (Outerbridge scores 0–1). Raman spectra were acquired with both the ball lens and convex lens. Subsequently, explants were diametrically cut in half. For one half, the topmost 500 μ m of cartilage was excised for GAG content analysis. Histological sections from the other half were analyzed for a modified-Mankin-based SOFG stain uptake score, based on percentage depletion per total area of unmineralized articular cartilage, as described.²⁵ Ball lens Raman GAG scores were compared to surface cartilage GAG content measures. Convex lens Raman GAG scores were compared to the SOFG stain uptake score. To illustrate Raman arthroscopy's ability to characterize the spatial variation in tissue composition along a contiguous joint surface, Raman GAG scores were acquired at discrete anatomical sites along the articular surface of an excised human femoral head specimen, obtained from a total hip arthroplasty procedure (50/♀; Kellgren–Lawrence grade 1). Raman GAG scores were acquired at three discrete anatomic sites along the articular surface and compared to corresponding Safranin O intensities.

2.6 | Polarized Raman probe assessment of zonal COL alignment ex vivo

We evaluated whether our polarized Raman probe could assess the loss of the SZ during cartilage degeneration. Full-thickness bovine explants were subjected to mechanical surface abrasion to remove sequential zonal layers ($n = 5$ explants per group): no abrasion (SZ intact), mild abrasion (exposing the MZ), and severe abrasion (exposing the DZ) (detailed methodology in Supporting Information Material). The parallel and perpendicular polarized Raman spectra ($n = 5$) were collected from each sample. The depolarization ratio (perpendicular/(parallel + x)) of each spectral set was calculated and used for input to a partial least squares–discriminant analysis (PLS-DA), with leave-one-out cross-validation. Orthogonal latent variables (LVs) were derived from Raman intensity peak positions highly associated with polarization-sensitive COL bands that maximized the covariance between spectral variation and abrasion group affinity.

2.7 | Raman probe cartilage thickness quantification ex vivo

For Raman thickness assessments, the cartilage layer of bovine osteochondral explants was variably excised to achieve chondral thicknesses ranging from 0.3 to 2.1 mm. Raman spectra were acquired via the convex lens to better detect the Raman spectra from

the subchondral bone through diffuse light scattering. Using known reference spectra of cartilage ECM (GAG, COL, H₂O) as well as bovine subchondral bone (Bone_{REF}; Figure S3) and its regression coefficient (Bone_{score}), multivariate linear regression was applied to the aggregate Raman spectra.

2.8 | Interanatomical variability as revealed by Raman spectroscopy ex vivo

We further assessed the capability of Raman biomarkers to predict properties of cartilage from different anatomical sites of the ovine knee joint, which exhibit biochemical and mechanical variability.²⁶ Raman probe measurements and mechanical testing were performed on osteochondral explants (Ø6.0 mm) from the medial and lateral femoral condyles, and tibial plateaus (1–2 explants per surface) of a skeletally mature ovine knee joint. The chondral layer of explants was subsequently analyzed for GAG content, H₂O content, and thickness. Univariate and multivariate regression using the compositional Raman scores were applied to predict biochemical contents, thickness, and elastic modulus.

2.9 | Raman arthroscopy for in situ and in vivo diagnostics

Confounding factors related to in situ intra-articular Raman diagnostic measurements were further assessed, including (1) interference from synovial fluid (SF), (2) sensitivity of Raman biomarkers to probe-to-cartilage surface incidence angle, and (3) acquisition time to achieve reliable Raman signal (all described in Supporting Information Material). Furthermore, in situ measurements of cartilage ECM composition were performed on intact ex vivo bovine antebrachio-carpal (wrist) joints before and after intra-articular enzymatic GAG depletion treatment using the Raman arthroscopy probe inserted intra-articularly through a 10-gauge hypodermic needle trocar (Supporting Information Material).

In vivo Raman arthroscopy was approved by the University of Pennsylvania Veterinary School IACUC. Raman spectra were collected from the distal femoral condyle articular cartilage of a live skeletally mature sheep via a mini arthrotomy of the stifle joint.

3 | RESULTS

3.1 | Raman probe GAG quantification ex vivo

Chemical treatments induced a stepwise depletion of GAG from cartilage explants (Figure 2A). COL content (mean: $4.4 \pm 0.9\%$ per wet weight [%ww]) and H₂O content (mean: $86.7 \pm 2.6\%$ ww) were minimally altered by these treatments. Concomitant with chemically induced GAG depletion was a prominent decrease in Raman signal intensity in the ranges 1000–1100 and 1200–1300 cm^{-1} (Figure 2B).

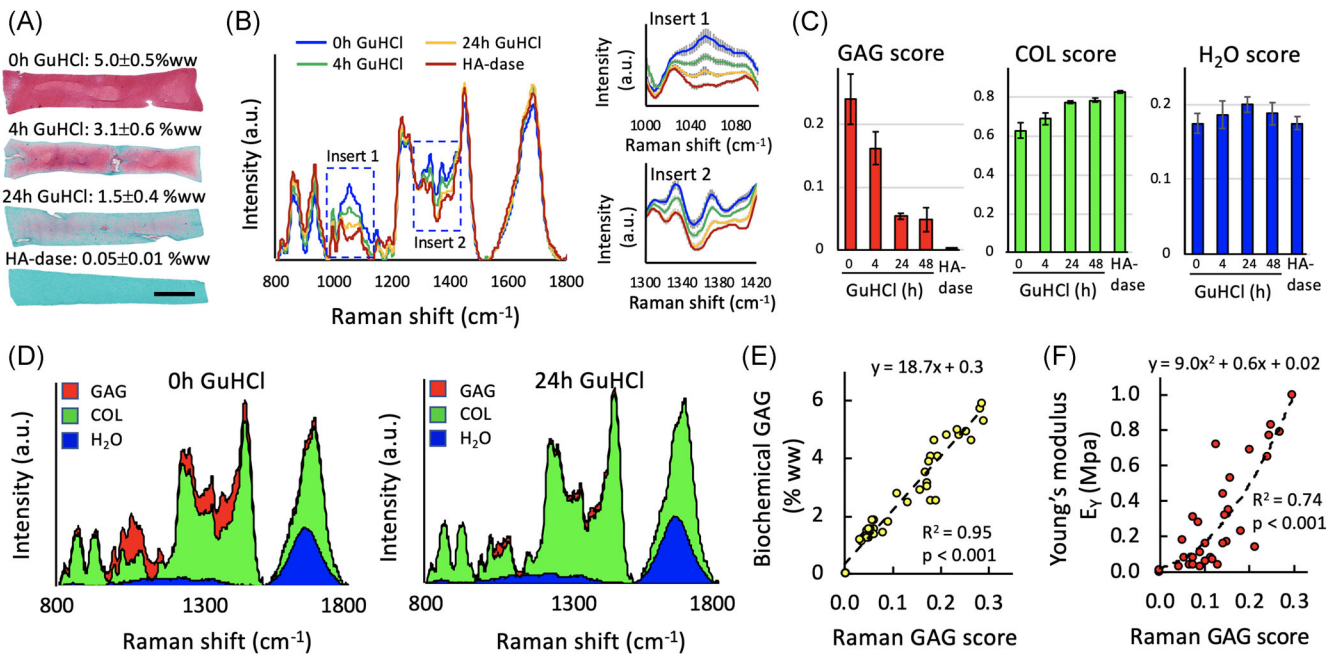


FIGURE 2 Raman probe glycosaminoglycan (GAG) measurements. (A) Guanidine hydrochloride (GuHCl) and hyaluronidase (HA-dase)-induced GAG depletion of cartilage explants (Safranin O histology and DMBB-measured GAG levels). Scale bar = 1 mm. (B) GuHCl/HA-dase-induced decrease of measured Raman probe spectra intensity at 1000–1100 and 1300–1450 cm⁻¹ wavenumbers (mean ± standard deviation). (C) Regression coefficients (scores) for GAG, collagen (COL), and H₂O from multivariate linear regression decomposition of Raman spectra for GuHCl/HA-dase timed exposure groups. (D) Two-dimensional stacked area graph showing the cumulative contribution of GAG, COL, and H₂O spectra to composite Raman cartilage spectra after multivariate linear regression decomposition. GAG spectral contribution attenuated after GAG depletion by GuHCl, while COL and H₂O contributions were relatively unaffected. Bivariate regression between Raman GAG scores versus (E) assay-measured GAG content and (F) compressive Young's modulus (E_y) for explants [Color figure can be viewed at wileyonlinelibrary.com]

Following multivariate regression analysis (Equation 1), the Raman GAG score decreased in proportion to the reduction of GAG from the explants; the Raman scores for COL and H₂O were less affected (Figure 2C). The cumulative spectral contribution of the individual ECM constituents accounted for 94% of the variation of the composite cartilage spectra (Figure 2D; $R^2 = 0.94 \pm 0.01$; $p < 0.001$). The GAG scores predicted 95% of the variation in measured tissue GAG content (Figure 2E; $R^2 = 0.95$; $p < 0.001$; Table S1) and 74% of the variation in the measured compressive modulus (E_y) for all explants (Figure 2F; $R^2 = 0.74$; $p < 0.001$), demonstrating the capacity of our Raman probe to predict progressive GAG loss and mechanical softening of hyaline cartilage associated with OA.

3.2 | Raman probe depth selective GAG quantification ex vivo

The ball lens and convex lens exhibited different DOP values as verified by the Raman signal attenuation of polystyrene substrates under varying thickness cartilage layers (Figure 3A). Cartilage explants exhibited progressive surface GAG depletion with increasing trypsin treatment time (Figure 3B). Raman GAG scores deduced from Raman spectra obtained through the surface-targeting ball lens

predicted 86% of the GAG tissue content (Figure 3C; $R^2 = 0.86$; $p < 0.001$; Table S2). However, Raman GAG scores deduced from spectra obtained through the deep focus convex lens, only predicted 40% of the GAG content ($R^2 = 0.4$; $p < 0.001$; Table S2); GAG scores were influenced by residual GAG remaining in the DZ, due to restricted diffusion of the GAG-depleting enzyme. Raman GAG scores from the ball lens further predicted 86% of the elastic modulus (Figure 3D; $R^2 = 0.86$; $p < 0.001$). These results indicate that Raman arthroscopy with a surface-focusing lens is advantageous for quantification of cartilage surface GAG depletion and softening.

3.3 | Raman probe GAG quantification in human cartilage ex vivo

Human chondral explants exhibited a range of Safranin O staining intensities and GAG contents (Figure 4A). The ball-lens-acquired GAG scores predicted 66% of the variation of GAG content in the topmost 500 μ m tissue layer (Figure 4B; $R^2 = 0.66$; $p < 0.001$; Table S3). Convex-lens-acquired GAG scores predicted 53% of the variation of a SOFG stain uptake score (Figure 4C; $R^2 = 0.53$; $p < 0.01$; Table S3). Raman GAG scores were acquired at discrete anatomic sites along the articular surface of an excised human femoral head (Figure 4D,E). Low Raman

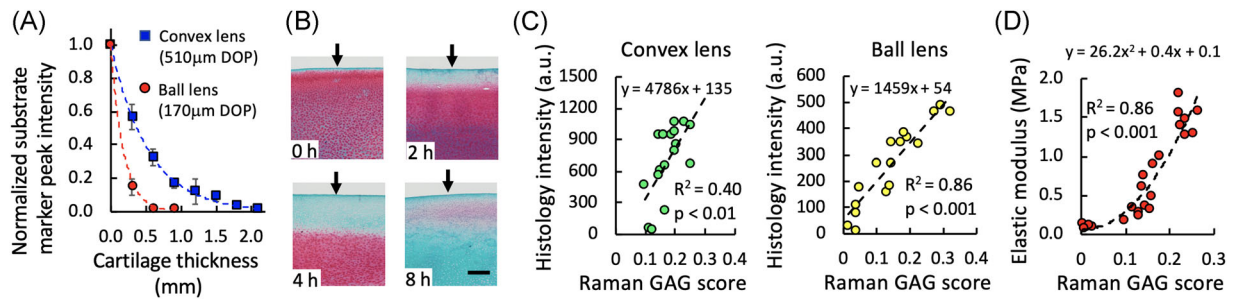


FIGURE 3 Raman probe depth selective measurements. (A) Lens-specific depth of penetration (DOP) based on measured decay of polystyrene substrate Raman signal under variable cartilage thickness layers (Supporting Information Data). (B) Representative Safranin O sections depicting trypsin-induced glycosaminoglycan (GAG) depletion from the articular surface of cartilage explants. Scale bar = 250 µm. (C) Bivariate linear regression between Raman probe-measured GAG scores and colorimetric Safranin O-measured GAG content for deep focusing convex lens and surface-targeting ball lens. (D) Bivariate linear regression between ball lens measured GAG scores and indentation elastic modulus [Color figure can be viewed at wileyonlinelibrary.com]

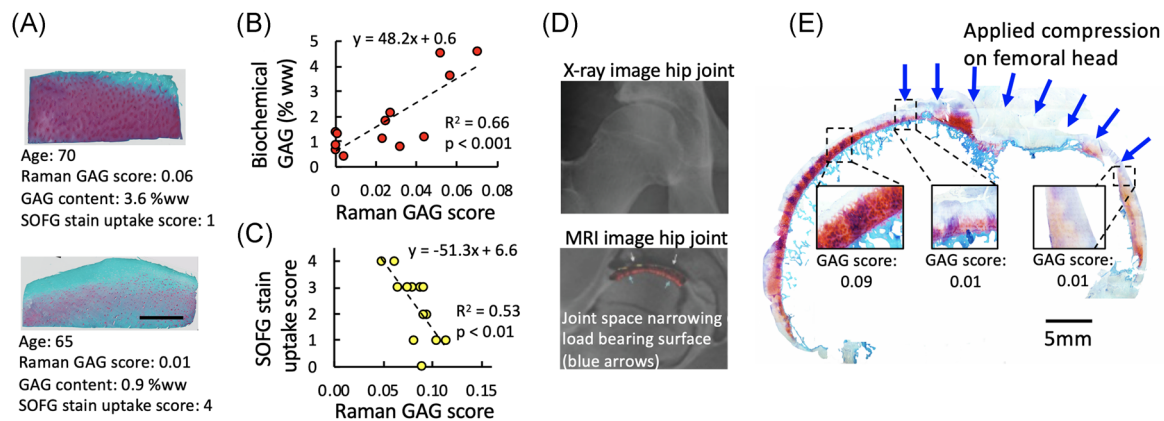


FIGURE 4 Raman probe glycosaminoglycan (GAG) measurements in human cartilage ex vivo. (A) Representative Safranin O histological sections of GAG-replete and GAG-depleted cartilage explants from human autopsy donors along with Raman GAG scores, GAG content, and Safranin O–fast green (SOFG) stain uptake score. Scale bar = 1 mm. (B) Bivariate linear regression between Raman probe GAG scores (ball lens measured) and DMMB-measured GAG content of $n = 13$ human explants ex vivo. (C) Bivariate linear regression between Raman probe GAG scores (convex lens measured) and SOFG stain uptake scores. (D) Representative radiographic and magnetic resonance imaging (MRI) sagittal plane images of the arthritic hip joint, illustrating joint space narrowing at superior femoral head, corresponding to a load-bearing region of the hip during standing. (E) Raman probe GAG scores were acquired at discrete anatomic regions along with a sagittal slice of a human femoral head articular joint surface ex vivo. GAG scores reflect the depletion of GAG and cartilage thinning observed on MRI and histological section [Color figure can be viewed at wileyonlinelibrary.com]

GAG scores were observed in the GAG-depleted hyaline cartilage, comprising the loaded region of the hip joint, while high GAG scores were observed in the GAG-replete hyaline cartilage comprising the unloaded region of the hip joint.

3.4 | Polarized Raman probe for assessment of zonal COL alignment

Consistent differences between the perpendicular and parallel polarization spectra were observed among the groups (no abrasion, mild abrasion, and severe abrasion) at Raman intensity peak positions highly associated with polarization-sensitive COL bands: 861, 930, 1257, 1448, and 1654 cm^{-1} (Figure 5A).²⁷ The depolarization ratio

spectra (i.e., intensity ratio between the perpendicular and parallel components of the Raman scattered light) revealed that differences in the polarized Raman spectra portrayed the varied zonal organization of the COL fiber network (Figure 5B). From PLS-DA, LV loadings LV1 and LV2 demonstrated good discriminatory separation among the abrasion groups (Figure 5C) and incorporated diagnostically relevant spectral variations that reflected the integrity of the SZ COL network (LV1: 10.36% and LV2: 6.48%; Figure 5D). Compared to LV1, LV2 better-differentiated samples where the SZ was intact ($p < 0.001$), therefore, LV2 was used as a Raman collagen alignment factor (RCAF) to depict the extent that SZ COL was retained (Figure 5E). These results show that COL alignment and SZ degeneration can be quantified by taking advantage of the polarization response of cartilage.

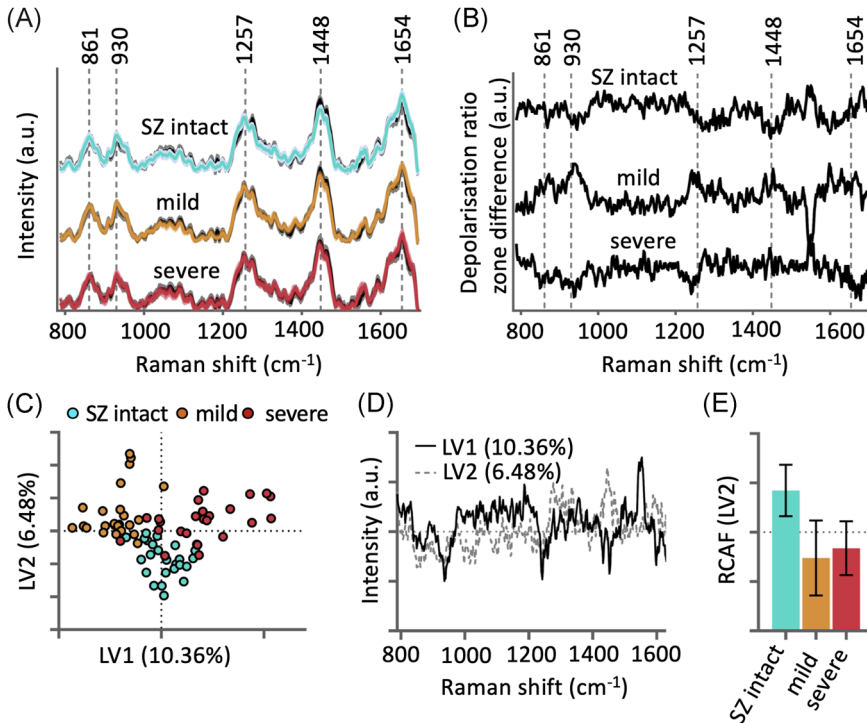


FIGURE 5 Polarized Raman probe collagen alignment measurements. (A) Mean polarized Raman spectra (perpendicular [color lines] and parallel [black lines]) of cartilage with an intact superficial zone (SZ), mild abrasion, and severe abrasion of the surface layer. (B) Difference spectra of the polarization ratio (parallel/perpendicular) reveal differences in Raman spectra due to the integrity of SZ collagen. (C) Partial least squares–discriminant analysis (PLS-DA) scores show good separation of the different erosion groups. (D) PLS-DA latent variable (LV) loadings LV1 and LV2. (E) Raman collagen alignment factor (RCAF) for detecting the extent of SZ abrasion corresponding to LV2 [Color figure can be viewed at wileyonlinelibrary.com]

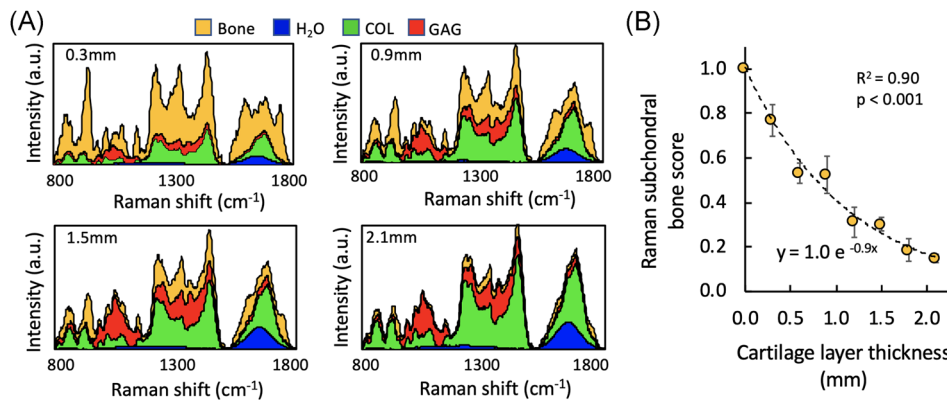


FIGURE 6 Raman probe cartilage thickness measurements. (A) Two-dimensional stacked area graph showing the contribution of glycosaminoglycan (GAG), collagen (COL), H₂O, and subchondral bone to composite Raman cartilage spectra after multivariate linear regression decomposition for osteochondral cartilage explants with a 0.3, 0.9, 1.5, and 2.1 mm thick cartilage layer. (B) Bivariate regression between Raman probe measured subchondral bone score versus cartilage layer thickness [Color figure can be viewed at wileyonlinelibrary.com]

3.5 | Raman probe cartilage thickness quantification ex vivo

Following multivariate regression analysis of the Raman spectra of variable thickness bovine osteochondral explants, the contribution of bone signal to the aggregate spectra decreased with increasing cartilage thickness (Figure 6A). The regression coefficient for the subchondral bone contribution (bone score) to the cumulative Raman spectra varied inversely with thickness of the chondral layer, following an exponential decay function (Figure 6B). The bone score predicted 90% of the variability in cartilage thickness (Table S4).

3.6 | Interanatomical variability as revealed by Raman spectroscopy ex vivo

For ovine osteochondral explants (Figure 7A), the Raman GAG score predicted 96% of the GAG content ($p < 0.001$; Figure 7B), H₂O score predicted 85% of the water content ($p = 0.01$; Figure 7C), and bone score predicted 78% of the thickness ($p = 0.02$; Figure 7D). While GAG score alone predicted 80% of indentation modulus ($p = 0.02$; Figure 7E), multivariate regression using a linear combination of the Raman scores for GAG and H₂O predicted 94% of the indentation modulus ($p < 0.01$; Figure 7F).

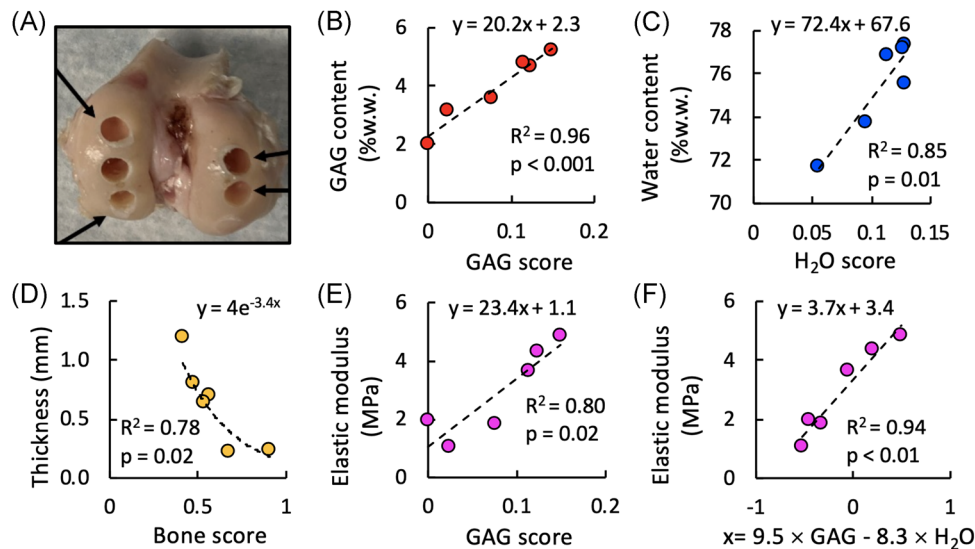


FIGURE 7 Raman probe interanatomical measurements of cartilage ex vivo. (A) Representative cored regions on ovine femoral condyle articular surfaces. Bivariate regression between (B) Raman glycosaminoglycan (GAG) score and GAG content, (C) Raman H₂O score and water content, (D) Raman bone score and cartilage thickness, and (E) Raman GAG score and elastic modulus. (F) Multivariate regression between a linear combination of Raman GAG and H₂O scores ($9.5 \times \text{GAG}_{\text{score}} - 8.3 \times \text{H}_2\text{O}_{\text{score}}$), and elastic modulus [Color figure can be viewed at wileyonlinelibrary.com]

3.7 | Raman arthroscopy in situ and in vivo diagnostics

Assessments of potential confounding factors related to in situ Raman arthroscopy measurements demonstrated that: (1) Raman biomarkers were insensitive to the presence of SF (Figure S4a), (2) 20° variation from a normal (90°) probe incidence angle to the cartilage surface had no significant effect on Raman biomarkers ($p < 0.05$; Figure S4b), and (3) integration time did not significantly affect measured Raman biomarkers (Figure S4c), indicating Raman arthroscopy measurements obtained in as little as 0.5 s will not compromise diagnostic capability. Furthermore, for intra-articular Raman arthroscopy assessments on intact wrist joints, Raman GAG scores were reduced by 75% after trypsin treatment corresponding to an 86% reduction in cartilage GAG content (Figure S5).

The distal femoral condyle articular cartilage of a live skeletally mature sheep was accessed via a mini arthrotomy of the stifle joint (Figure 1). The Raman needle probe was placed in gentle contact with the articular surface of the femoral condyle under image guidance. Raman spectra were acquired over a 10 s integration time to obtain the highest SNR for this in vivo demonstration. High-quality Raman spectra were acquired in vivo (Figure 1D), akin to ex vivo measures. The cumulative spectral contribution of the individual ECM constituents and subchondral bone derived by multivariate regression analysis accounted for 86% of the variation in the composite spectra (Figure 1E; Raman scores: GAG = 0.16, COL = 0.58, H₂O = 0.11, subchondral bone = 0.10; $R^2 = 0.86$; $p < 0.001$). In vivo scores were similar to those obtained ex vivo on ovine osteochondral explants (Figure 7). This demonstration highlights the feasibility of in vivo Raman arthroscopy by

demonstrating successful compositional quantification in vivo and the ability to maneuver the needle probe in a surgical setting.

4 | DISCUSSION

We present a novel needle-based arthroscopic platform for achieving real-time, polarized Raman spectroscopy quantification of changes in cartilage composition, structure, and material properties associated with OA. Using ex vivo bovine models of OA, aging human cartilage explants, and anatomical site-varied ovine cartilage explants, we demonstrate that our Raman arthroscopic probe can measure biomarkers that accurately predict changes in GAG content and COL disorganization associated with the degradation of hyaline cartilage in OA. A critical innovation, described herein, is the implementation of multivariate regression to ascertain the contribution of individual spectra corresponding to the ECM constituents GAG, COL, H₂O, and bone to the cumulative Raman cartilage spectra.^{24,28} The derived regression coefficient biomarkers (GAG scores) account for 95% of the variation of the GAG content of enzymatically depleted bovine explants, 66% of the GAG variation in human chondral explants, and 94% of the GAG variation in ovine osteochondral explants. In addition, the derived Raman H₂O and COL scores can reveal damage to the integrity of the tensile COL matrix that gives rise to cartilage swelling in OA.²⁹ Raman biomarkers can further be used to predict cartilage mechanical properties. Raman GAG scores account for 86% of the variation of the elastic modulus of GAG depleted bovine explants. For healthy native ovine cartilage specimens, the multivariate combination of Raman-derived biomarkers (GAG and H₂O score) accounts for 94% of the cartilage elastic modulus. This demonstration

highlights the important capability of composite Raman biomarkers to provide assessments of tissue functional material properties.

A potential limitation of this analysis is that purified reference chemicals may exhibit spectral profiles that are different from ECM *in situ*, thus contributing to variance in regression models. Future models may improve Raman assessments by accounting for the compositional and organizational complexities of ECM constituents *in situ*. The lower GAG score correlation exhibited for human specimens likely results from the spatial disparity between the tissue regions of interest analyzed with the Raman probe and biochemical assays—an effect that is likely more pronounced for these heterogeneous specimens. Future validations may benefit from the use of direct ECM measurement techniques with a higher spatial resolution that can offer more faithful comparisons with biomarkers acquired within the penetration depth of the Raman probe.

To further evaluate the zone-dependent, anisotropic microstructure of the COL matrix, we incorporated polarized Raman spectra into our platform to exploit differences between the perpendicular and parallel polarization spectra. This novel functionality, achieved by tightly focusing the distal ball lens to avoid bulk tissue polarization scrambling, enables assessment of the alignment and organization of the SZ COL matrix. To maximize diagnostically relevant spectral variations that reflect the integrity of the SZ COL, PLS-DA was applied to the depolarization spectra, giving rise to LVs (LV1 and LV2) that incorporated Raman intensity peak positions highly associated with polarization-sensitive COL bands. LV2 efficiently discriminates an intact SZ and can therefore be used as an alignment factor to depict the extent that SZ COL was retained.

While the diagnosis of surface GAG and COL loss requires utilization of a ball lens that collects Raman signal predominantly from the topmost cartilage regions, Raman cartilage thickness measurements may require a deep focusing lens to collect sufficient Raman signal from the subchondral bone. Thus, the lens configuration selected depends on the diagnostic metric to be quantified. For immature bovine specimens, to resolve Raman-based cartilage thickness, we used a large, needle-free lens to target the subchondral bone. In future iterations of our device, an interchangeable deep tissue lens (hemispherical lens or custom manufactured high DOP microlens) will be incorporated into the needle probe.

To demonstrate the feasibility of translating Raman needle arthroscopy to the clinic, we acquired high-quality Raman spectra of articular cartilage comprising the ovine femoral condyle *in vivo*, which proved to be similar to *ex vivo* assessments. Clinical translation is further supported by establishing: (1) Raman spectra can be obtained in as little as 0.5 s, (2) the derived Raman GAG scores are insensitive to the presence of SF, and (3) the probe incidence angle can vary up to 20° from normal to the cartilage surface without compromising diagnostic accuracy. Furthermore, *in situ* intra-articular Raman spectra acquired on intact bovine diarthrodial joints before and after enzymatic-induced degradation validated that Raman GAG scores were consistent with measured GAG content.

There has been growing interest in Raman spectroscopy as a potential OA diagnostic technology, building upon prior work on IR

spectroscopy.^{30–32} Prior *ex vivo* studies have examined Raman spectral changes in explanted late-stage OA cartilage tissues^{20–22,33} or cartilage subjected to mechanical damage.^{16–18} With the exception of Unal et al.,³³ who used high-wavenumber Raman peak ratios to measure cartilage water content but not GAG or COL, prior Raman assessments have consisted of univariate peak analysis or principal component analysis, which do not provide quantification of biochemical or structural tissue changes relevant to the tissue's functional performance. Furthermore, with the exception of Esmonde-White et al.,¹⁹ who used a probe to measure cartilage erosion, previous Raman investigations have been performed on benchtop microscopy systems that are incompatible with *in situ* intra-articular Raman evaluations. Our study represents the first *in vivo* Raman diagnostic investigation to utilize a clinically compatible needle arthroscopic probe to measure biomarkers that are associated with the pathognomonic changes of OA: GAG depletion, SZ COL loss, erosion (thinning), and swelling (increased hydration). In future work, we can incorporate additional key molecular constituents into spectral decomposition models (e.g., GAG/COL subtypes, lipids, crosslinks, DNA), thus providing additional biomarkers to potentially improve diagnostics on specimens with increased compositional complexity.

This study supports the use of our Raman probe as a transformative diagnostic platform for objective monitoring of treatment outcomes of emerging OA therapies. It can be employed over the hierarchy of cartilage tissue model systems, including (1) *in vitro* nondestructive, repeated-measure assessments of the efficacy of novel OA therapeutics in ameliorating degeneration of live explant tissues, and (2) *in vivo* assessments (preclinical and clinical) as a minimally invasive, real-time diagnostic tool for articular cartilage disease stage and evaluation of treatment response. Future *in vivo* investigations will be required to directly ascertain the capability of Raman arthroscopy to monitor degeneration and repair. Raman arthroscopy can complement other state-of-the-art and emerging OA diagnostic platforms (MRI [T1 ρ , dEGEMRIC],^{34,35} ultrasound,³⁶ contrast-enhanced computed tomography [CT],³⁷ OCT,³⁸) in portraying changes in cartilage composition, structure, and material properties. While the current diagnostic gold standard, MRI, is non-invasive and can image the entire joint, it is limited by spatial resolution of the cartilage surface,³⁹ systemic administration of potentially toxic contrast agents,⁴⁰ extended imaging times, expense, lack of portability, and/or infrastructure requirements. Alternatively, Raman arthroscopy can serve as a low-cost, minimally invasive, portable diagnostic platform that achieves rapid and safe (no radiation or toxic contrast agent exposure) assessments of cartilage composition. While Raman arthroscopy is limited to point-based measures, it can be interfaced with image guidance (e.g., Arthrex NanoScope) to achieve targeted assessments of specific anatomical sites. Raman biomarkers appear to be more sensitive to changes in cartilage composition than MRI (T1 ρ relaxation times account for approximately 20% of cartilage GAG variation⁴¹), although direct comparisons will need to be performed in future work. As such, Raman can potentially lead to the development of clinical trials that incorporate fewer participants, shorter durations, and patient cohorts with earlier stages of OA

(before irreversible degeneration has transpired)—together, improving the likelihood of the identification of chondroprotective OA therapies. Raman arthroscopy may further provide a unique utility for diagnostics of joints with characteristic thin cartilage layers (e.g., shoulder, elbow) where image-based cartilage evaluation is particularly limited.

In the future, Raman needle arthroscopy can be performed as a cost-effective, point-of-care office procedure capable of diagnosing the early stages of OA before irreparable changes in cartilage biochemical and biophysical properties are evident radiographically. Raman arthroscopic screening can be performed on patient populations known to be at high risk for developing OA as a consequence of traumatic joint injury, physical occupations, internal derangement, obesity, joint malalignment, and genetic predisposition. The periodic monitoring of cartilage biomarkers may allow for the timely prescription of emerging chondroprotective therapies, such as biologics, viscosupplements, lifestyle changes (weight loss, activity cessation), physical therapy, or surgical reconstruction. As such, our Raman arthroscopy platform can set the foundation for the identification of novel OA therapies and subsequently support their administration in the clinic.

ACKNOWLEDGMENTS

The authors thank Dr. Thomas Schaer for assistance with in vivo ovine measures, Joshua Auger for assistance with procurement and processing of human cartilage specimens, and Sedat Dogru and Chenhao Yu for their assistance in implementing mechanical testing protocols. This study was supported by the Musculoskeletal Transplant Foundation (MTF) Biologics, the Arthritis Foundation, the 2020 Boston University Materials Science & Engineering Innovation Award, the Clare-Booth Luce Scholars Program, the Boston University Undergraduate Research Opportunities Program, the Boston University College of Engineering Distinguished Summer Research Fellowship and Summer Term Alumni Research Scholars Program, and the European Research Council (ERC) under the European Union's Horizon 2020 Research and Innovation Programme (Grant No. 802778).

CONFLICT OF INTERESTS

The authors declare that there are no conflict of interests.

AUTHOR CONTRIBUTIONS

Michael B. Albro, Mads S. Bergholt, Brian D. Snyder, and Mark W. Grinstaff designed and supervised the study, interpreted the data, and wrote the paper. Kimberly R. Kroupa, Man I Wu, Juncheng Zhang, and Wei Wong performed Raman measurements, analyzed Raman data, and performed biochemical analysis. Magnus Jensen performed polarized Raman measurements. Julie B. Engiles performed histological analyses. All authors contributed to scientific discussions and the preparation of the manuscript.

ORCID

Mark W. Grinstaff  <https://orcid.org/0000-0002-5453-3668>

Michael B. Albro  <https://orcid.org/0000-0002-3071-0252>

REFERENCES

- Lawrence RC, Felson DT, Helmick CG, et al. Estimates of the prevalence of arthritis and other rheumatic conditions in the United States. Part II. *Arthritis Rheum.* 2008;58(1):26-35.
- Hunter DJ, Bierma-Zeinstra S. Osteoarthritis. *Lancet.* 2019;393(10182):1745-1759.
- Venn M, Maroudas A. Chemical composition and swelling of normal and osteoarthrotic femoral head cartilage. I. Chemical composition. *Ann Rheum Dis.* 1977;36(2):121-129.
- Krishnan R, Kopacz M, Ateshian GA. Experimental verification of the role of interstitial fluid pressurization in cartilage lubrication. *J Orthop Res.* 2004;22(3):565-570.
- Temple-Wong MM, Bae WC, Chen MQ, et al. Biomechanical, structural, and biochemical indices of degenerative and osteoarthritic deterioration of adult human articular cartilage of the femoral condyle. *Osteoarthritis Cartilage.* 2009;17(11):1469-1476.
- Pritzker KP, Gay S, Jimenez SA, et al. Osteoarthritis cartilage histopathology: grading and staging. *Osteoarthritis Cartilage.* 2006;14(1):13-29.
- Raub CB, Hsu SC, Goldberg I, et al. eds. Degeneration of human femoral condyle articular cartilage involves changes in collagen network orientation and anisotropy. Paper presented at: Orthopaedic Research Society Annual Meeting; 2012.
- Maier F, Lewis CG, Pierce DM. The evolving large-strain shear responses of progressively osteoarthritic human cartilage. *Osteoarthritis Cartilage.* 2019;27(5):810-822.
- Goldring MB, Goldring SR. Osteoarthritis. *J Cell Physiol.* 2007;213(3):626-634.
- Messier SP, Callahan LF, Beavers DP, et al. Weight-loss and exercise for communities with arthritis in North Carolina (we-can): design and rationale of a pragmatic, assessor-blinded, randomized controlled trial. *BMC Musculoskelet Disord.* 2017;18(1):91.
- Roos EM, Dahlberg L. Positive effects of moderate exercise on glycosaminoglycan content in knee cartilage: a four-month, randomized, controlled trial in patients at risk of osteoarthritis. *Arthritis Rheum.* 2005;52(11):3507-3514.
- Lohmander LS, Hellot S, Dreher D, et al. Intraarticular sprifermin (recombinant human fibroblast growth factor 18) in knee osteoarthritis: a randomized, double-blind, placebo-controlled trial. *Arthritis Rheumatol.* 2014;66(7):1820-1831.
- Webb D, Naidoo P. Viscosupplementation for knee osteoarthritis: a focus on Hylan G-F 20. *Orthop Res Rev.* 2018;10:73-81.
- Huang BJ, Hu JC, Athanasiou KA. Cell-based tissue engineering strategies used in the clinical repair of articular cartilage. *Biomaterials.* 2016;98:1-22.
- Raman CV, Krishnan KS. A new type of secondary radiation. *Nature.* 1928;121:501-502.
- Dehring KA, Crane NJ, Smukler AR, McHugh JB, Roessler BJ, Morris MD. Identifying chemical changes in subchondral bone taken from murine knee joints using Raman spectroscopy. *Appl Spectrosc.* 2006;60(10):1134-1141.
- Lim NS, Hamed Z, Yeow CH, Chan C, Huang Z. Early detection of biomolecular changes in disrupted porcine cartilage using polarized Raman spectroscopy. *J Biomed Opt.* 2011;16(1):017003.
- Tong L, Hao Z, Wan C, Wen S. Detection of depth-depend changes in porcine cartilage after wear test using Raman spectroscopy. *J Biophotonics.* 2018;11(4):e201700217.
- Esmonde-White KA, Esmonde-White FW, Morris MD, Roessler BJ. Fiber-optic Raman spectroscopy of joint tissues. *Analyst.* 2011;136(8):1675-1685.
- Takahashi Y, Sugano N, Takao M, Sakai T, Nishii T, Pezzotti G. Raman spectroscopy investigation of load-assisted microstructural alterations in human knee cartilage: preliminary study into diagnostic potential for osteoarthritis. *J Mech Behav Biomed Mater.* 2014;31:77-85.

21. Kumar R, Grønhaug KM, Afseth NK, et al. Optical investigation of osteoarthritic human cartilage (ICRS grade) by confocal Raman spectroscopy: a pilot study. *Anal Bioanal Chem.* 2015;407(26):8067-8077.
22. de Souza RA, Xavier M, Manguiera NM, et al. Raman spectroscopy detection of molecular changes associated with two experimental models of osteoarthritis in rats. *Lasers Med Sci.* 2014;29(2):797-804.
23. Jensen M, Horgan CC, Vercauteren T, Albro MB, Bergholt MS. Multiplexed polarized hypodermic Raman needle probe for biostructural analysis of articular cartilage. *Opt Lett.* 2020;45(10):2890-2893.
24. Albro MB, Bergholt MS, St-Pierre JP, et al. Raman spectroscopic imaging for quantification of depth-dependent and local heterogeneities in native and engineered cartilage. *NPJ Regen Med.* 2018;3:3.
25. McIlwraith CW, Frisbie DD, Kawcak CE, Fuller CJ, Hurtig M, Cruz A. The OARSI histopathology initiative - recommendations for histological assessments of osteoarthritis in the horse. *Osteoarthritis Cartilage.* 2010;18(suppl 3):S93-S105.
26. Risch M, Easley JT, McCready EG, et al. Mechanical, biochemical, and morphological topography of ovine knee cartilage. *J Orthop Res.* 2021;39(4):780-787.
27. Jensen LK, Eenberg W. Occupation as a risk factor for knee disorders. *Scand J Work Environ Health.* 1996;22(3):165-175.
28. Bergholt MS, Albro MB, Stevens MM. Online quantitative monitoring of live cell engineered cartilage growth using diffuse fiber-optic Raman spectroscopy. *Biomaterials.* 2017;140:128-137.
29. Maroudas A, Venn M. Chemical composition and swelling of normal and osteoarthrotic femoral head cartilage. II. Swelling. *Ann Rheum Dis.* 1977;36(5):399-406.
30. West PA, Bostrom MP, Torzilli PA, Camacho NP. Fourier transform infrared spectral analysis of degenerative cartilage: an infrared fiber optic probe and imaging study. *Appl Spectrosc.* 2004;58(4):376-381.
31. Palukuru UP, Hanifi A, McGoverin CM, Devlin S, Lelkes PI, Pleshko N. Near infrared spectroscopic imaging assessment of cartilage composition: validation with mid infrared imaging spectroscopy. *Anal Chim Acta.* 2016;926:79-87.
32. Prakash M, Joukainen A, Tornaiainen J, et al. Near-infrared spectroscopy enables quantitative evaluation of human cartilage biomechanical properties during arthroscopy. *Osteoarthritis Cartilage.* 2019;27(8):1235-1243.
33. Unal M, Akkus O, Sun J, et al. Raman spectroscopy-based water content is a negative predictor of articular human cartilage mechanical function. *Osteoarthritis Cartilage.* 2019;27(2):304-313.
34. Taylor C, Carballido-Gamio J, Majumdar S, Li X. Comparison of quantitative imaging of cartilage for osteoarthritis: T2, T1rho, dGEMRIC and contrast-enhanced computed tomography. *Magn Reson Imaging.* 2009;27(6):779-784.
35. Bashir A, Gray ML, Hartke J, Burstein D. Nondestructive imaging of human cartilage glycosaminoglycan concentration by MRI. *Magn Reson Med.* 1999;41(5):857-865.
36. Kortekaas MC, Kwok WY, Reijnen M, Huizinga TW, Kloppenburg M. Osteophytes and joint space narrowing are independently associated with pain in finger joints in hand osteoarthritis. *Ann Rheum Dis.* 2011;70(10):1835-1837.
37. Bansal PN, Joshi NS, Entezari V, et al. Cationic contrast agents improve quantification of glycosaminoglycan (GAG) content by contrast enhanced CT imaging of cartilage. *J Orthop Res.* 2011;29(5):704-709.
38. Nebelung S, Brill N, Müller F, et al. Towards optical coherence tomography-based elastographic evaluation of human cartilage. *J Mech Behav Biomed Mater.* 2016;56:106-119.
39. Stubendorff JJ, Lammentausta E, Struglics A, Lindberg L, Heinegård D, Dahlberg LE. Is cartilage sGAG content related to early changes in cartilage disease? Implications for interpretation of dGEMRIC. *Osteoarthritis Cartilage.* 2012;20(5):396-404.
40. Perazella MA. Current status of gadolinium toxicity in patients with kidney disease. *Clin J Am Soc Nephrol.* 2009;4(2):461-469.
41. Li X, Cheng J, Lin K, et al. Quantitative MRI using T1rho and T2 in human osteoarthritic cartilage specimens: correlation with biochemical measurements and histology. *Magn Reson Imaging.* 2011;29(3):324-334.

SUPPORTING INFORMATION

Additional Supporting Information may be found online in the supporting information tab for this article.

How to cite this article: Kroupa KR, Wu MI, Zhang J, et al. Raman needle arthroscopy for in vivo molecular assessment of cartilage. *J Orthop Res.* 2022;40:1338-1348.
<https://doi.org/10.1002/jor.25155>